Effects of Molecular Structure on Segment Orientation in Siloxane Elastomers. 1. NMR Measurements from Compressed Samples

Ronald C. Hedden, Evan McCaskey, Claude Cohen,* and T. M. Duncan

Olin Hall, School of Chemical Engineering, Cornell University, Ithaca, New York 14853

Received October 11, 2000

ABSTRACT: ^{2}H NMR spectral data are reported for two types of compressed, deuterium-labeled siloxane elastomers: ^{2}H-labeled poly(diethylsiloxane) (PDES) networks and ^{2}H-labeled poly(dimethylsiloxane) (PDMS) free chains dissolved at low concentration in PDES host networks. We find that compressed PDES networks have higher segment orientation under stress than PDMS networks, a result that follows partially from the larger segment size (persistence length) of PDES. The internal motions of PDES chain segments are found to be substantially less isotropic than in PDMS, which leads to larger ^{2}H NMR line widths. Chain segments in compressed PDES elastomers have enhanced orientation compared to predictions from excluded-volume calculations. The ^{2}H NMR spectral splitting for compressed PDES networks is not directly proportional to $(\lambda^2 - \lambda^{-1})$, unlike the case of conventional elastomers. The behavior of the compressed PDES networks is tentatively attributed to an enthalpic orientational coupling between PDES segments.

Introduction and Background

^{2}H NMR spectroscopy is sensitive to bond orientation and dynamics through the deuterium quadrupolar interaction, so it can provide a wealth of useful information about segment-level orientation in polymeric materials.[1−10] Current ^{2}H NMR work seeks to establish the relationship between molecular structure and the macroscopic response of elastomers under deformation. In this work, we report spectra for novel siloxane elastomers under compression, noting the effects of chemical structure on segment orientation.

Previously, we characterized partially deuterated PDMS (poly(dimethylsiloxane)) probe chains in PDMS networks by ^{2}H NMR.[11,12] NMR spectra were obtained for three types of deuterated probe chains: (1) elastic network chains, (2) pendent chains, and (3) free chains dissolved in the network. At a given compression, the segment orientation in the probe chains was approximately the same for all three chain types. These studies demonstrated that segment orientation is induced primarily by excluded-volume interactions with neighboring chains, at least for PDMS.

The physical basis for these interactions is still a matter of investigation. Excluded-volume (entropic) interactions and enthalpic interactions have both been suggested as contributors to segment alignment.[1,2,9,13] However, experimental evidence has shown[4,10,12,14] that an enthalpic interaction alone cannot satisfactorily explain segment orientation, particularly for free probe chains in a host network. The recent theory of Brereton and Ries[1] focuses instead on excluded-volume interactions to explain probe chain orientation and has been more successful in explaining experimental observations.[12,15] In Brereton and Ries' model, the effects of network and probe chain chemical structure are introduced through molecular parameters such as segment length, screening length, molecular weight, and interaction parameters.

In this study, we extend the experimental work on segment orientation in elastomers by studying networks of poly(diethylsiloxane), PDES. Compared to PDMS, PDES has a higher chain stiffness (as measured by persistence length)[16] because the larger ethyl side groups influence the preferred chain conformations. The dynamics of segment motion in PDES melts[17,18] (previously studied by NMR) also differ substantially from PDMS. One reason for studying the PDES networks is therefore to note the effects of chain stiffness and dynamics on the deformation-induced segment orientation. A second reason we chose to study these networks is their demonstrated ability to undergo a remarkable strain-induced phase transition. In uniaxial extension, initially amorphous PDES elastomers can spontaneously change to an aligned mesomorphic state under appropriate conditions of temperature and molecular weight between cross-links.[19,21,22] A stable mesophase can also be observed in PDES melts of molar mass larger than 28 kg/mol.[23] Because we have not observed this transition in compressed PDES networks, the mesophase itself will not play a large role in the current paper. However, the ability to form an aligned mesophase (with the penalty of losing configurational entropy) demonstrates that strong enthalpic interactions exist that favor alignment of the siloxane chain segments in PDES. In this work, we demonstrate that such enthalpic interactions affect the relationship between the molecular structure and the compression ratio.

In the current work, we measure the effects of chemical structure on segment orientation by comparing ^{2}H NMR spectra of PDES and PDMS networks. Two types of experiments are conducted. In the first set of experiments, we observe spectra for partially deuterated PDMS free chains dissolved in compressed PDES networks. The concentration of free PDMS is kept very low so that secondary effects due to probe chain concentration can be neglected. Combination of these results with the previous work on PDMS networks allows quantitative analysis of the spectral data in terms of Brereton and Ries' model. In the second set of experiments, PDES networks with elastic chains labeled with $-CD_2CH_3$ groups are studied.

10.1021/ma0017541 CCC: $20.00
Published on Web 04/13/2001

Table 1. Characteristics of PDES Polymer Chains Used as Network Precursors

polymer batch	ethyl group	fraction	M_n (kg/mol)	M_w/M_n
PDES-d_2-1[a]	$-CD_2CH_3$ (5%)	a	18.3	1.34
		b	14.5	1.24
		c	11.8	1.19
		d	10.2	1.15
		e	8.2	1.15
PDES-d_2-2[a]	$-CD_2CH_3$ (25%)	a	38.3	1.32
		b	25.6	1.22
		c	19.9	1.21
		d	17.4	1.17
PDES-3[a]	$-CH_2CH_3$ (100%)	a	34.5	1.41
		b	25.7	1.28
		c	22.9	1.23
		d	20.8	1.22
		e	16.0	1.18
		f	9.8	1.19
PDES-4[a]	$-CH_2CH_3$ (100%)		9.8	1.8
PDES-5[b]	$-CH_2CH_3$ (100%)		3.7	1.22
PDES-6[b]	$-CH_2CH_3$ (100%)		10.6	1.46

[a] Prepared by cationic polymerization with trifluoromethanesulfonic acid. [b] Prepared by polymerization with NaOH/12-crown-4 catalyst/promoter.

Experimental Procedures

Synthesis of Deuterated PDMS. The 25% deuterated PDMS was synthesized as described previously.[11,12] The chains had $M_w = 15$ kDa, and $M_w/M_n = 1.40$.

Synthesis of Deuterated PDES. To simplify the ^{2}H NMR spectra, we produced PDES with only one type of deuteron. We chose to use materials containing $-CD_2CH_3$ ethyl groups rather than CH_2CD_3, because we are interested in the orientation of the polymer backbone segments, and the deuterons in $-CD_2CH_3$ are more closely coupled to the Si−O backbone. To synthesize the deuterated monomer hexaethyl(*1,1-d*$_2$)cyclotrisiloxane, we started from ethyl(*1,1-d*$_2$) alcohol (Aldrich) and synthesized ethyl(1,1-d$_2$) iodide by a standard reaction.[24] Next, we prepared diethyl(*1,1-d*$_2$)dichlorosilane by a method analogous to that previously employed to make di(methyl-*d*$_3$)-dichlorosilane.[25] Hexa(ethyl-*1,1-d*$_2$)cyclotrisiloxane was prepared by reaction of a mixture of diethyl(*1,1-d*$_2$)dichlorosilane and nondeuterated diethyldichlorosilane (Gelest, Inc.) with zinc oxide as previously described.[19,26,27]

Two batches of monomer were produced: one approximately 5% deuterated and one approximately 25% deuterated. To make the nondeuterated form of the monomer, we started from commercial nondeuterated diethyldichlorosilane. The monomers were vacuum distilled at least two times over freshly crushed calcium hydride (Alfa Aesar, 88−96%) before polymerization. Repeated monomer purification improved the degree of end group functionalization in the polymerization reaction.

Deuterated poly(diethylsiloxane) containing $-CD_2CH_3$ groups, hereafter called PDES-*d*$_2$, was prepared by cationic polymerization of the deuterated monomer in the presence of trifluoromethanesulfonic acid.[19,27,29] The batches were labeled PDES-*d*$_2$-1 (5% D) and PDES-*d*$_2$-2 (25% D). Two other batches of nondeuterated PDES labeled PDES-3 and PDES-4 were used in this work and were also prepared by this technique. The chains were α,*ω*-vinyl-end-capped for later use in end-linking reactions. The raw polymers were then fractionated with toluene/methanol to reduce the polydispersity. By fractionation, we obtained several "network precursor" samples from the original batches, with varying molecular weights. PDES-4 was used without prior fractionation to make some imperfect networks.

To obtain α,*ω* vinyl-terminated PDES short chains, two samples of PDES were prepared by the NaOH/12-crown-4 catalyst/promoter system[27,28] with relatively short polymerization times. These samples, labeled PDES-5 and PDES-6, were not fractionated because they had reasonably low values of M_w/M_n.

Network precursor characteristics are listed in Table 1.

PDES Networks. Networks were prepared from the vinyl-functionalized PDES chains by a technique previously refined (for PDMS) by Patel et al.[30] Hydrosilylation end-linking was accomplished with tetrakis(dimethylsiloxy)silane (Gelest, Inc.) as a cross-linker and *cis*-dichlorobis(diethyl sulfide)platinum-(II) (Strem Chemicals, Inc.) as a catalyst. Table 2 lists the networks.

The samples were cast into sheets with smooth surfaces and uniform thickness (1.25 mm) by use of a glass mold. Samples for dynamic mechanical analysis and NMR compression experiments were cut from the sheets with a razor blade or "cookie cutter" device. The uniform thickness of the samples was important for obtaining accurate compression ratios in NMR experiments.

Soluble materials were extracted from the networks by toluene as previously described.[30] The final network thus consisted of only elastic and pendent chains, with no free chains or dissolved impurities. The soluble fractions and equilibrium swelling ratios Q in toluene are reported in Table 2.

Networks with soluble fractions of around 1% or less were assumed to have a minimal amount of structural defects. The 25% deuterated networks (Opt-*d*$_2$-1 to Opt-*d*$_2$-5) in Table 2 met this criterion and will hereafter be called optimal networks. The 5% deuterated networks (Imp-*d*$_2$-1 to Imp-*d*$_2$-8) had higher soluble fractions and are hereafter called imperfect networks. The nondeuterated networks consisted of both optimal (Opt-1 to Opt-6) and imperfect (Imp-1 to Imp-9) samples.

Further details on monomer, polymer, and network synthesis can be found in ref 27.

Dissolution of Deuterated PDMS Probe Chains in Nondeuterated PDES Networks. Nondeuterated PDES networks with deuterated PDMS free chains were prepared by soaking the extracted PDES networks in a 25% deuterated PDMS melt between 3 and 7 days. These samples are hereafter denoted as "PDMS-in-PDES". The sample was wiped clean after removing it from the PDMS and was allowed to equilibrate at room temperature for several days before running any NMR experiments. The weight fraction of the PDMS free chains in the PDES networks was determined by NMR spectral intensity calibrated by a PDMS liquid reference sample. The weight fraction was less than 1 wt % in all cases, due to the poor miscibility of PDES and PDMS. Leaving the network samples in the PDMS for longer periods did not significantly increase the PDMS weight fraction. The low weight fraction of PDMS in the samples caused difficulties with the signal-to-noise ratio of the NMR spectrum, but working near the limit of infinite probe chain dilution simplified the analysis of the spectral data.

Network Modulus Measurements. The elastic (Young's) moduli of the PDES networks were measured on a Perkin-Elmer DMA 7e in uniaxial extension at 25 °C at a strain of approximately 1%. The elastic moduli were converted to equilibrium shear moduli, G_e, through the previously established[31] relationship $E = 3G_e$. The cross-sectional area of a sample was assumed not to change appreciably under the small strains studied. The measured moduli of the dry networks are reported in Table 2.

^{2}H NMR Instrumentation. Spectra were obtained on a Bruker CXP200 spectrometer operating at a frequency of 30.721 MHz for deuterium. A Bruker z32vHP probe body with a custom-built probe head and coil were used. The coil had a diameter of 1.2 cm, length of 3 cm, and approximately 15 turns. With this coil, the probe circuit had a quality factor of about 95.

The networks were compressed uniaxially by a custom-built compression cell previously described.[12] The sample could be compressed uniformly by tightening two screws simultaneously. The final thickness of the sample was determined by inserting hard plastic spacers of known thickness into the compression cell. Network samples typically measured 3.5 mm × 5 mm × 1.25 mm. The compression cell was oriented in the coil such that the compression axis was parallel to the applied magnetic field.

Table 2. PDES Networks

sample	polymer precursor	G_e/RT (mol/m^3)	M_c (kg/mol)	Q in toluene	W_{sol} (wt %)
		Optimal Networks			
Opt-d_2-1	PDES-d_2-2a	76.8	12.9	3.71	0.4
Opt-d_2-2	PDES-d_2-2b	79.1	12.5	3.65	
Opt-d_2-3	PDES-d_2-2c	77.4	12.8	3.69	
Opt-d_2-4	PDES-d_2-2d	85.8	11.5	3.49	0.5
Opt-d_2-5	PDES-d_2-2e	92.1	10.7	3.36	1.0
Opt-1	PDES-3a	75.5	13.1	3.93	0.3
Opt-2	PDES-3b	73.6	13.5	3.90	1.1
Opt-3	PDES-3c	69.2	14.3	4.02	1.2
Opt-4	PDES-3d	78.5	12.6	3.76	1.0
Opt-5	PDES-3f	99.3	9.97	3.33	1.4
Opt-6	PDES-5	143.0	4.30	2.56	3.6
		Imperfect Networks			
Imp-d_2-1	PDES-d_2-2a	56.0	17.7	4.45	3.6
Imp-d_2-2	PDES-d_2-2a	52.3	18.9	4.56	3.9
Imp-d_2-3	PDES-d_2-2b	51.0	19.4	4.53	4.6
Imp-d_2-4	PDES-d_2-2b	44.7	22.2	4.95	
Imp-d_2-5	PDES-d_2-2c	42.9	23.1	5.06	6.5
Imp-d_2-6	PDES-d_2-2c	41.0	24.2	5.19	6.9
Imp-d_2-7	PDES-d_2-2c	59.1	16.8	4.27	4.1
Imp-d_2-8	PDES-d_2-2d	56.2	17.6		
Imp-1	PDES-3d	71.9	13.8	3.81	
Imp-2	PDES-3e	84.2	11.8	3.49	
Imp-3	PDES-3e	82.8	12.0	3.53	
Imp-4	PDES-3e	64.8	15.3	4.07	
Imp-5	PDES-3e	43.6	22.7	5.06	
Imp-6	PDES-6	48.1	20.6	4.90	9.4
Imp-7	PDES-3f	95.7	10.3	3.17	1.5
Imp-8	PDES-4	40.3	24.6	5.11	9.5
Imp-9	PDES-4	44.7	22.2	4.86	8.1

A slip condition at the elastomer−compression cell interface was assumed. In practice, the slip condition was not strictly met, and the elastomer bulged somewhat at the sides, most notably at high compression ratios. In our analysis, we have assumed that the slightly uneven compression had a negligible effect on the observed spectral splittings. In subsequent experiments at high degrees of deformation, we noted some broadening and distortion of the line shapes, which may have been due in part to uneven compression. We will return to this issue in the Discussion section.

In the experiments with PDMS free chains dissolved in PDES networks, high compression sometimes partially expelled the probe chains from the host network. When the host network was saturated with free chains, the increase in the osmotic pressure in the sample caused by compression was enough to expel some PDMS. Because we assume probe concentration does not affect the spectral splitting at low concentrations, this phenomenon did not affect our analysis. A small central peak in the ^{2}H NMR spectrum was sometimes observed due to this leakage. The problem could be circumvented by compressing the sample to the highest strain to be studied and leaving it overnight. The expelled chains could then be wiped from the elastomer surface before acquiring a spectrum. We still observed a small central peak in many of our spectra that we attribute to a small amount of free chains on the outside of the sample. In general, this peak did not interfere with the data analysis.

^{2}H NMR Pulse Programs. In the case of the PDMS free chains dissolved in PDES networks, a simple $(90°)_x$ pulse was found to be adequate (typical duration 11 μs). The delay between scans was typically 1 s. Because of the small concentration of deuterium in some samples, a large number of transients (10 000−100 000) were typically required to achieve a reasonable signal-to-noise ratio in the final spectrum. To improve the apparent signal-to-noise ratio, a line broadening of 10 Hz was added to each spectrum by multiplying the free induction decay by an exponential function.

In the case of the deuterated PDES networks, the $(90°)_x$ pulse was used for the majority of the experiments. Some spectra were taken with the standard spin-echo sequence $(90°)_x-\tau-(180)_y-\tau$ to reduce broadening due to magnetic field inhomogeneities. However, the PDES spectra had some components with very short transverse relaxation times, which would be attenuated if τ was too large. Thus, the simple $(90°)_x$ pulse was preferred. A line broadening of 50 Hz was added to the spectra in this case.

Results and Discussion

Data Analysis: Calculation of the ^{2}H NMR Spectral Splittings. The observed ^{2}H NMR spectra of compressed elastomers exhibit a doublet.[2−12] The spectral feature of greatest interest is the "splitting" or separation between the two peaks. Determination of the spectral splitting was not always straightforward, especially when the peaks overlapped. Each spectrum was least-squares fit to a pair of identical components, and the separation between the maxima was used to calculate the splittings objectively.

In a typical spectrum of deuterated PDMS probe chains in a PDES network, the two peaks were quite sharp and symmetrical. The spectrum was assumed to be the sum of a pair of identical Lorentzian functions with different centers. The program iterated on the peak widths, the center of the pair, and the splitting until the best fit was obtained. The experimental line shapes fit well to a pair of Lorentzian functions (Figure 1).

For the deuterated PDES networks, some spectral broadening was observed, and the resulting spectra could not be modeled by a single pair of Lorentzian functions. The observed line shapes were inconsistent with a recently published analytical expression[32] for the spectra of strained networks. However, we discovered that the spectral data could be (empirically) well represented by a sum of two Lorentzian pairs constrained to have the same center. Typically, the pair with the larger splitting had the larger broadening. The shape of a typical calculated spectrum can be seen from Figure 2. Although the mathematical form chosen to represent the spectra was empirical, it was a satisfac-

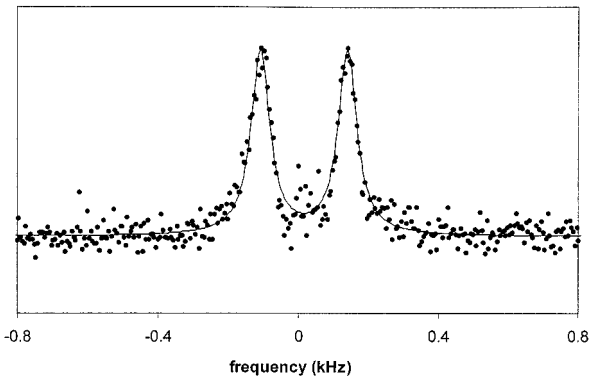

Figure 1. ^{2}H NMR spectrum of PDMS free chains in a compressed PDES network (sample Imp-5, $\lambda = 0.54$) fitted to a pair of identical Lorentzian functions.

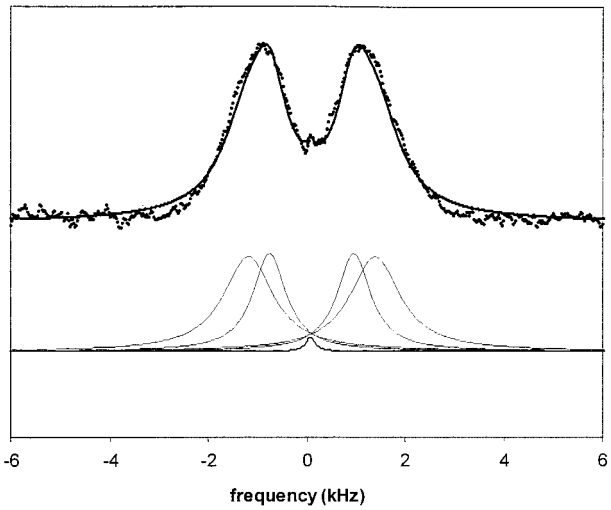

Figure 2. Decomposition of a representative PDES spectrum into component peaks (sample Opt-d_2-1, $\lambda = 0.64$). Top: Experimental data and total fitted spectrum. Bottom: calculated left, right, and central peaks.

tory vehicle for decomposing the spectra into left and right peaks.

The splitting was defined as the separation between the maxima of the fitted doublet components. We explored an alternative method in which the splitting was based on the centers of mass of the left and right peaks. However, the centers of mass were influenced significantly by the outer edges of the spectra, which were sensitive to an arbitrary contribution from the phase correction and baseline correction routines.

In some PDES compression spectra, a small third peak was observed near the center. This peak usually had a fractional area of less than 1% of the total spectrum and often had an irregular or inconsistent shape. Although we neglect this peak in the data analysis, it was included in the fitting algorithm as a single Lorentzian peak.

Dependence of the Spectral Splittings on Compression Ratio. Case 1: Deuterated PDMS in Nondeuterated PDES Networks (PDMS-in-PDES). Spectra were obtained as a function of compression ratio, $\lambda = L/L_0$, where L_0 was the thickness of the uncompressed sample (approximately 1.25 mm), for 12 samples with varying moduli. At low compression (λ near unity), separation of the spectra into component peaks was dubious, because the peaks were not clearly resolved. Therefore, few splittings are reported in the

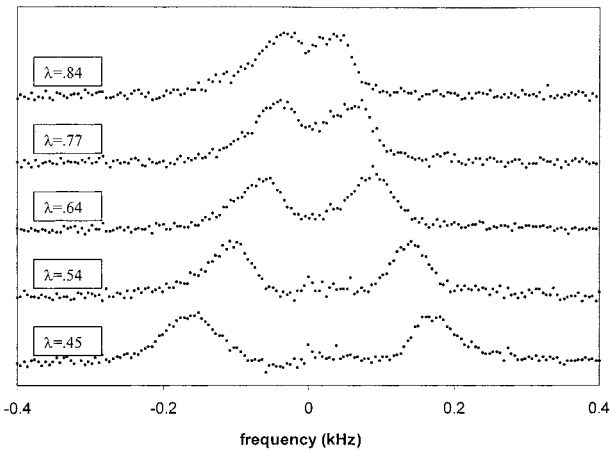

Figure 3. ^{2}H NMR spectra of PDMS free chains in a PDES network (sample Imp-5) as a function of compression ratio for $\lambda = 0.84$, 0.77, 0.64, 0.54, and 0.45.

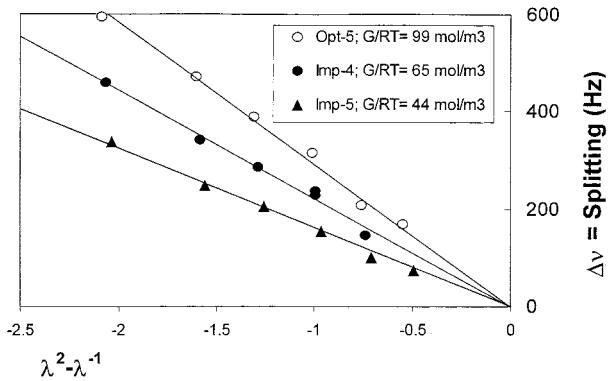

Figure 4. Dependence of the splitting $\Delta\nu$ on $(\lambda^2 - \lambda^{-1})$ for PDMS probe chains (25% ^{2}H-labeled, $M_w = 15\,000$ g/mol) in compressed PDES networks.

range $0.8 < \lambda < 1$. At very high deformations ($\lambda < 0.4$), the network samples generally cracked or shattered, so this was the practical lower limit for the compression ratio. It was possible to satisfactorily analyze spectra over the range $0.4 < \lambda < 0.8$.

Sample spectra for PDMS probes in network Imp-5 ($G_e/RT = 44$ mol/m^3) are shown in Figure 3. In the uncompressed samples, a single peak was observed (not shown), which split into an overlapping doublet upon slight compression. As the compression ratio λ decreased (i.e., deformation increased), the separation between the component peaks increased. The width of the peaks also gradually increased, and the shape distorted slightly for some samples at high λ. Line shapes and response to compression were similar to results previously reported for deuterated PDMS networks.[12]

The spectral splittings formed a straight line through the origin when plotted as $\Delta\nu$ vs $(\lambda^2 - \lambda^{-1})$, in accordance with the predictions of Brereton and Ries' model.[1] The same behavior has been noted experimentally for deuterated PDMS networks[3,12] and for PDMS free chains dissolved in PDMS networks.[12] Figure 4 shows $\Delta\nu$ vs $(\lambda^2 - \lambda^{-1})$ for three selected samples. The slopes of these lines, called "strain efficiencies," are the primary experimental parameters linking segment orientation to deformation. Strain efficiencies were calculated for each data set based on least-squares fits to straight lines forced to pass through the origin. (For the sake of clarity, we plotted only three data sets in Figure 4, choosing the ones with the least amount of scatter.

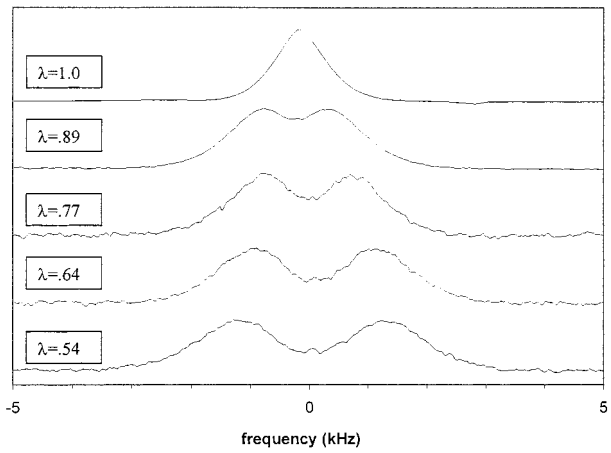

Figure 5. ^{2}H NMR spectra of a PDES network (sample Opt-d_2-1) as a function of compression ratio for $\lambda = 1.0$, 0.89, 0.77, 0.64, and 0.54.

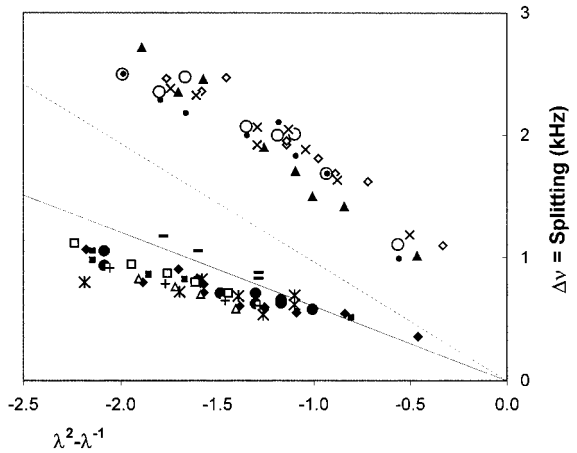

Figure 6. Observed ^{2}H NMR peak splittings and model predictions for compressed PDES networks. Optimal samples: Opt-d_2-1 (◇); Opt-d_2-2 (×); Opt-d_2-3 (•); Opt-d_2-4 (○); Opt-d_2-5 (▲). Imperfect samples: Imp-d_2-1 (●); Imp-d_2-2 (∗); Imp-d_2-3 (■); Imp-d_2-4 (◆); Imp-d_2-5 (+); Imp-d_2-6 (△); Imp-d_2-7 (−); Imp-d_2-8 (□). Solid line: prediction for $G_e/RT = 50$ mol/m^3. Dashed line: prediction for $G_e/RT = 80$ mol/m^3.

Although the other data sets showed more scatter,[27] all the data for PDMS probes in PDES networks could be satisfactorily fitted to a line passing through the origin.)

The data in Figure 4 at high deformations ($\lambda^2 - \lambda^{-1} < -1.5$) do not deviate from the linear trend established at low deformation. Therefore, we conclude that the uneven compression had a minimal effect on the calculated splittings.

Case 2: Deuterated PDES Networks. Corresponding spectra were obtained as a function of compression ratio for PDES networks with deuterated elastic chains. Figure 5 shows spectra for optimal network Opt-d_2-1 ($G_e/RT = 77$ mol/m^3) as a function of compression ratio.

The spectrum of a typical optimal PDES network at $\lambda = 1$ (no compression) consisted of a single peak with a full width at half-height on the order of 1 kHz. The corresponding spectral width previously observed for optimal PDMS networks with comparable moduli (such as sample A-1 in ref 11) was on the order of 0.2−0.4 kHz. The difference in widths reflects the fact that there is comparatively less motional averaging of the deuterium quadrupolar interaction when the deuteron is attached to a methylene group of a PDES chain.

For $\lambda < 1$, the left and right component peaks of the PDES spectra exhibited non-Lorentzian line shapes. The observed line shape is a convolution of (1) the line shape corresponding to a motionally averaged methylene at a given average segment orientation and (2) the segment orientation distribution function. We attribute the non-Lorentzian line shape to a skewed distribution of segment orientations within the PDES networks. On the basis of the narrow, symmetrical peaks obtained from PDMS probe chains in PDES networks, we rule out the possibility that uneven compression caused the non-Lorentzian distribution of orientations. The PDES network chains have a markedly different distribution of averaged C−D bond orientations compared to the PDMS probe chains.

The mesophase transition was not observed in our PDES compression experiments. The ^{2}H NMR spectrum of the mesophase segments has a distinctive splitting of 19.1 kHz in networks[20] and 19 kHz in melts,[18] and no such peaks were observed in any of our compression spectra. Thus, the non-Lorentzian shape of the doublet components in our PDES spectra was not due to the presence of multiple phases.

The reason that our compressed PDES networks did not transform into the mesophase can be understood from the mesophase microstructure. The mesophase has a columnar structure in which the Si−O chain backbones align in a common direction (the axes of the columns).[33] In uniaxial extension, the mesophase can form because the chains are stressed in a common direction. In compression (which can be represented as a biaxial extension), the chain backbones orient with radial symmetry in a plane normal to the compression axis. While segments may align with each other on a local basis, it is not possible for all the chain backbones to align in a common direction.

The calculated PDES spectral splittings were plotted as a function of ($\lambda^2 - \lambda^{-1}$) in Figure 6. The data in Figure 6 constitute two distinct groups: the optimal networks with $G_e/RT \approx 80$ mol/m^3 and the imperfect networks with $G_e/RT \approx 50$ mol/m^3 (see Table 2 for individual values). The splittings were not linear with respect to ($\lambda^2 - \lambda^{-1}$). Because of the nonlinearity of the data, it was not meaningful to calculate strain efficiencies.

The relationship between $\Delta\nu$ and ($\lambda^2 - \lambda^{-1}$) indicates that segments in PDES respond differently to stress than do more typical networks such as PDMS. The difference in properties between PDES and PDMS is due to the difference in segment−segment interactions in the two polymers. It has been suggested that segment alignment is energetically favorable in PDES because overlap of ethyl groups on neighboring chain segments is maximized when the siloxane backbones are oriented in a common direction.[16,33,38] The orientational enthalpic coupling between segments in PDES arises as nonpolar ethyl groups associate with each other in preference to the polar Si−O backbone. Alignment of the chain backbones decreases the internal energy of the network, a result that has been verified by calorimetric measurements.[21,22,39−42] For the mesophase transition to be spontaneous, this favorable decrease of internal energy must offset the entropic penalty for alignment. The entropy change associated with mesophase formation[33] is small (<1 kJ/mol), lending credibility to these ideas. In PDMS, the interaction between methyl groups may not be strong enough to permit an aligned mesophase to form. In addition, alignment of the more flexible PDMS macromolecules might require a larger conformational entropy decrease relative to PDES.

Irrespective of the thermodynamic details, PDES chain segments have a greater propensity to orient with their neighbors than PDMS chain segments do. This is manifested in two features of the NMR spectra: the stronger couplings between segments in PDES increases the splitting in stressed samples, and the limited motional averaging of the deuterium quadrupolar interaction in PDES leads to comparatively broader ^{2}H NMR line shapes.

Given the physical properties of PDES, the broadening of the doublet components may be due to favorable enthalpic interactions between PDES segments on neighboring chains. Such interactions may be present in many types of elastomers, but it is clear that PDES is a special case where the interaction between segments is quite important. If this explanation is correct, then predicting segment orientation based on excluded-volume effects alone will be insufficient to completely describe the orientation process in PDES. In the analysis section of this work, we demonstrate that this is in fact the case.

Analysis of the PDMS and PDMS-in-PDES NMR Splittings Using the Model of Brereton and Ries. The NMR line splittings for (1) PDMS networks and (2) PDMS-in-PDES networks were interpreted in terms of molecular parameters according to the recent theory of Brereton and Ries.[1] In the case of a network with deuterated elastic chains, the strain efficiencies, p, are related to molecular parameters via the relationship

$$p \equiv \frac{\Delta\nu_A}{\lambda^2 - \lambda^1} = \frac{-\Delta_A}{\pi} \tag{1}$$

where $\Delta\nu_A$ is the ^{2}H NMR line splitting from the network elastic chains and

$$\Delta_A = \left(\frac{2}{15\pi}\frac{1}{cb^3}\right)\left(\frac{b}{\xi}\right)_A {v_Q}^A \frac{1}{N_A} \tag{2}$$

In eq 2, c is the total concentration of monomer units, b is the root-mean-square end-to-end distance of a statistical segment, and ξ is the Edwards screening length.[34] N_A is the average number of statistical segments per elastic chain. v_Q (v_0 in ref 1) is the deuterium quadrupolar interaction constant, rescaled to account for any fast molecular motions within a statistical segment. The right-hand side of eq 1 contains a factor of -1 that arises in compression experiments because $(\lambda^2 - \lambda^{-1})$ is negative.

In this work, we take the quantity $1/cb^3$ to be unity for the entire data series. M_c, the molecular weight between effective cross-links, is calculated from the measured moduli G_e/RT of the elastomers as[35]

$$M_c = \frac{\rho RT}{G_e} \tag{3}$$

where ρ is the mass density (kg/m^3) of the dry host network.

The average number of segments per elastic chain, N_A, is then calculated as

$$N_A = \frac{M_c}{m_s} \tag{4}$$

where m_s is the molar mass of a statistical segment and has been previously determined to be about 640 g/mol for PDMS via computer simulation.[36] m_s is related to the root-mean-square segment length b through

$$b\ (\text{nm}) = (n_s)^{0.5} l_u = \left(\frac{m_s}{M_{SU}}\right)^{0.5} l_u\ (\text{nm}) \tag{5}$$

where n_s is the number of monomers per segment and l_u is the projected length of a monomer unit along the fully extended chain axis, equal to 0.255 nm for poly(di-*n*-alkylsiloxane)s.[16] M_{SU} is the mass of a structural unit (monomer) (74.2 g/mol for ^{1}H PDMS and 102.2 g/mol for ^{1}H PDES). We have neglected in eq 5 a constant prefactor that is close to unity for poly(di-*n*-alkylsiloxane)s. This prefactor will affect the absolute value of b but will have no effect on our analysis.

For PDES, no value of the segment length is available, so we estimated ${m_s}^{PDES}$ from the simulated value of ${m_s}^{PDMS}$, accounting for the differences in chain stiffness and monomer molecular weight. By this logic, we estimate the segment mass ${m_s}^{PDES}$ as

$${m_s}^{PDES} \approx {m_s}^{PDMS}\left(\frac{{l_K}^{PDES}}{{l_K}^{PDMS}}\right)\left(\frac{{M_{SU}}^{PDES}}{{M_{SU}}^{PDMS}}\right) \tag{6}$$

where l_K's represent the Kuhn lengths of the polymers (1.56 nm for PDMS and 1.96 nm for PDES).[16] There is not a large difference in the Kuhn lengths of PDES and PDMS, and these polymers have the same chemical structure of the backbone. Hence, we will assume that the first-order estimate of eq 6 is a reasonable one. From eqs 5 and 6, and the values of m_s, M_{SU}'s, l_u, and l_k's, we get $b^{PDMS} = 0.75$ nm, $b^{PDES} = 0.84$ nm, and ${m_s}^{PDES} = 1100$ g/mol. For simplicity, we have neglected the slight changes in monomer formula weight when the chains are partially deuterated.

In the case of deuterated free chains in a compressed host network of differing chemical structure, the NMR splitting of the free chains is given by[1]

$$\Delta_B = \frac{2}{15\pi}\frac{{v_Q}^B}{N_A}\frac{c_A}{c}\frac{1}{cb^3}\left[\frac{b}{\xi} + \frac{c_B}{c}F_B(\chi_F, N_A, N_B, c_A, c_B)\right] \tag{7a}$$

Here, the subscript "B" corresponds to the free chains and the subscript "A" to the network chains. The correction term F_B accounts for enthalpic interactions between the two species (as an interaction parameter χ_F) and for the effects of free chain concentration. F_B is of order $(1/{N_B}^{0.5})$ in most cases and is small compared to b/ξ, which is order 1. In our study, the concentration of free PDMS chains in the host network is less than 1 wt % ($c_B/c < 0.01$), and in this case, F_B will be negligibly small.[1] Then eq 7a reduces to

$$\Delta_B = \left(\frac{2}{15\pi}\frac{1}{cb^3}\right)\left(\frac{b}{\xi}\right)_A {v_Q}^B \frac{1}{N_A} \tag{7b}$$

The ratio b/ξ corresponds to the host network chains, whereas the quadrupolar interaction constant corresponds to the deuterated species and is a property of the free chains.

The measured strain efficiencies for PDMS networks and PDMS-in-PDES networks provide enough information to estimate the parameter (b/ξ) for both PDMS and PDES. Experimental values of $-\Delta_A$ and $-\Delta_B$ $(=\pi\Delta\nu/(\lambda^2 - \lambda^{-1}))$ for PDMS networks and PDMS-in-PDES networks, respectively, are plotted vs $1/N_A$ in Figure 7

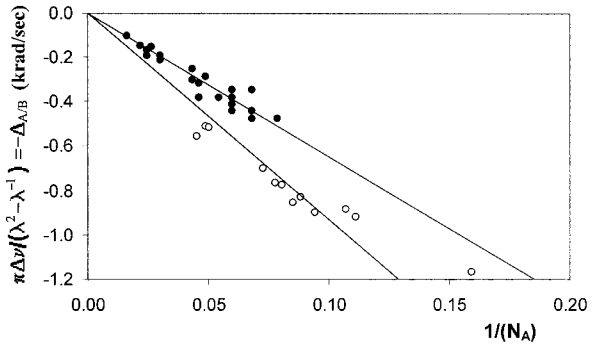

Figure 7. Analysis of measured strain efficiencies in terms of network structure: (●) PDMS networks (data from ref 12); (O) PDMS free chains in PDES host networks.

where N_A is calculated using eqs 3 and 4. The data for PDMS networks are from ref 12 and combine the results for elastic, pendent, and free probe chains. These data should lie on straight lines through the origin, according to eq 7b. Examining Figure 7, the data for PDMS networks do seem to follow the expected trend, at least over the modulus range studied. The PDMS-in-PDES network data can also be fitted to a line through the origin, except for the point at very high modulus (network Opt-6). Given the scatter in the data in Figure 7, it is not possible to say unambiguously whether the data in either series are truly linear. However, we will take the data to be linear to a first approximation.

Least-squares fits to the data in Figure 7 were calculated with a forced intercept of zero, yielding slopes of −6.46 krad/s for PDMS networks and −9.31 krad/s for PDMS-in-PDES networks. The datum point Opt-6 in the PDMS-in-PDES series was not included in the fit. Using eq 7b for the expression of the slope in Figure 7 for the PDMS networks, we find the following:

$$\left(\frac{b}{\xi}\right)_{\mathrm{PDMS}} {v_Q}^{\mathrm{PDMS}} = \left(\frac{15\pi}{2}\right)(6.46 \times 10^3) \qquad (8a)$$

We take the previously reported[1] value of ${v_Q}^{\mathrm{PDMS}} = 21$ kHz, which gives $(b/\xi)_{\mathrm{PDMS}} \approx 7$ from eq 8a.

For the deuterated PDMS free chains in PDES networks,

$$\left(\frac{b}{\xi}\right)_{\mathrm{PDES}} {v_Q}^{\mathrm{PDMS}} = \left(\frac{15\pi}{2}\right)(9.31 \times 10^3) \qquad (8b)$$

Combination of the results (8a) and (8b) gives

$$\left(\frac{b}{\xi}\right)_{\mathrm{PDES}} \approx 1.4\left(\frac{b}{\xi}\right)_{\mathrm{PDMS}} \qquad (9)$$

or $(b/\xi)_{\mathrm{PDES}} \approx 10$.

Qualitatively, we see from Figure 7 that PDMS free chains dissolved in PDES networks have ^{2}H NMR peak splittings larger than for PDMS chains in PDMS networks. Strained PDES networks are more efficient at orienting the segments of a PDMS probe chain. The result in eq 9 quantifies this observation; the higher network chain stiffness in PDES networks enhances excluded-volume effects, increasing the probe chain peak splitting by 40% compared to that of PDMS networks.

Calculation of the Reduced Quadrupolar Interaction in PDES. Figure 8 shows the decay of transverse magnetization vs time obtained from standard spin-echo experiments on four noncompressed PDES-d_2 networks with different moduli. Two optimal networks (Opt-d_2-1 and Opt-d_2-4) and two imperfect networks (Imp-d_2-1 and Imp-d_2-5) were chosen for these measurements. The experimental relaxation curves in Figure 8 were fitted to the approximate relationship[36,37]

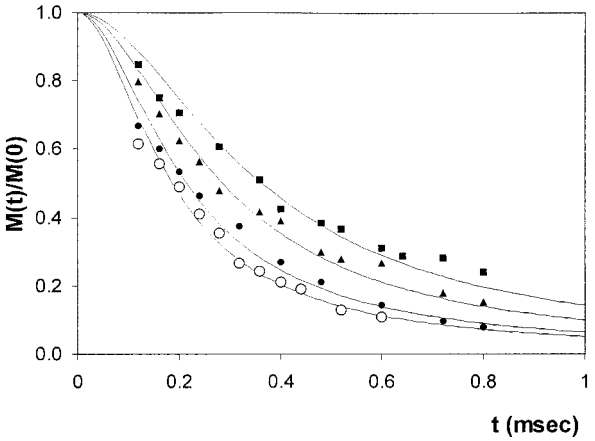

Figure 8. Transverse relaxation curves for uncompressed PDES-d_2 networks. Curves are fits to eq 10 for samples: Opt-d_2-4 (○); Opt-d_2-1 (●); Imp-d_2-1 (▲); Imp-d_2-5 (■).

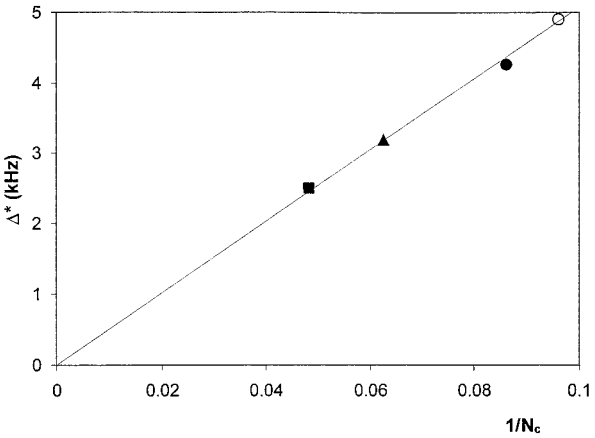

Figure 9. Fitted values of the time constant Δ* from transverse relaxation data of samples: Opt-d_2-4 (○); Opt-d_2-1 (●); Imp-d_2-1 (▲); Imp-d_2-5 (■).

$$M_t/M_0 = \mathrm{Re}\{(1 + i\Delta^* t)^{-1}(1 - 2i\Delta^* t)^{-1/2}\} \qquad (10)$$

The time constant Δ* is related to v_Q by

$$\Delta^* = 2v_Q/3N_c \qquad (11)$$

where N_c is the average number of statistical segments in an elastic chain. Equation 10 assumes that statistical segment dynamics are fast compared to the time scale $(v_Q)^{-1}$ set by the interaction constant. Figure 9 shows the calculated values of Δ* vs $1/N_c$ for the four samples studied, where N_c was calculated by eq 4. The dependence of Δ* vs $1/N_c$ is linear, with the slope = 51.1 kHz, giving ${v_Q}^{\mathrm{PDES}} = 76.6$ kHz.

The values of ${v_Q}^{\mathrm{PDMS}}$ and ${v_Q}^{\mathrm{PDES}}$ differ by a factor of 3.6. This result reflects the comparatively anisotropic segment motion in $-CD_2CH_3$ labeled PDES compared to $-CD_3$ labeled PDMS. The quadrupolar interaction is given (in frequency units) by

$$v_Q = \left(\frac{e^2qQ}{\hbar}\right)\overline{(3\cos^2\theta(t) - 1)} \equiv v_0\overline{(3\cos^2\theta(t) - 1)} \qquad (12)$$

where θ is the angle between the applied magnetic field and the electric field gradient at the site of the D nucleus, which is associated with local molecular structure (i.e., the C−D bond). The horizontal bar represents the time average of $\theta(t)$. e is the charge on a proton, q is the magnitude of the electric field gradient at the D nucleus, and Q is the electric quadrupole moment of the D nucleus. υ_0 is the quadrupolar interaction in the limit of zero molecular motion.

In the limit of rapid, isotropic molecular motion, the $\theta(t)$-dependent term in eq 12 averages to zero. In most polymers at room temperature, the averaging is incomplete, resulting in some residual quadrupolar interaction, υ_Q. In PDES, the effects of molecular motions within a segment average out the quadrupolar interaction less effectively than in PDMS. There is thus a difference in the time average of $(3\cos^2\theta(t) - 1)$ between the two polymers.

The monomer-level dynamics of PDES chains are clearly quite different from those of PDMS. The less efficient averaging of the quadrupolar interaction in PDES does not necessarily indicate slower bond-level dynamics but does indicate less isotropic dynamics despite the common Si−O backbone. This observation could indicate that orientational coupling forces in PDES are stronger than in PDMS. Alternately, the comparatively large size of the ethyl groups may restrict motion within a segment based purely on steric hindrance. Whatever the case, the anisotropic molecular dynamics within a PDES segment have pronounced effects upon the observed ^{2}H NMR line shape.

One result of incomplete motional averaging is the broadening of the component peaks in the spectra. For the samples used in this study, the line width of a PDES network spectrum was about 3−4 times larger than that of a PDMS network with comparable modulus. The effects that reduce the motional averaging also increases the observed splitting for a compressed elastomer, because according to eq 2, $\Delta\nu \propto \upsilon_Q$. Indeed, the observed splittings for our compressed PDES elastomers are much higher than for comparable PDMS elastomers: a few kilohertz for PDES (Figure 6) but only a few hundred hertz for PDMS.[11,12] Qualitatively, these observations seem to agree with the excluded-volume predictions of the theory of Brereton and Ries. However, in the analysis that follows, it will be shown that the quantitative dependence of the ^{2}H NMR line splitting in PDES cannot be predicted by excluded-volume arguments alone.

Analysis of the PDES-d_2 Spectral Data. Returning to Figure 6, it is seen that the spectral splittings for the deuterated PDES networks do not follow the same linear trend as the data for PDMS or PDMS-in-PDES networks. Rather, the spectral splitting increases rapidly at small deformations and then increases more slowly at high deformations. The curvature in the data of Figure 6 is less pronounced or absent for the imperfect samples but is quite obvious for the optimal networks. Regardless of the nonlinear shape of the curves in Figure 6, it is instructive to compare the data to the model predictions. Inserting the estimated values for υ_Q^{PDES} and $(b/\xi)_{PDES}$ leads to the model predictions shown in Figure 6. Here, we have calculated the predicted splittings for hypothetical elastomers with $G_e/RT = 50$ mol/m^3 (solid line) and $G_e/RT = 80$ mol/m^3 (dashed line), which correspond roughly to the average moduli for the imperfect and optimal data sets, respectively. The predictions of the model are reasonably close to the data for the imperfect networks but underpredict the splittings of the optimal networks considerably.

A Proposed Enthalpic Orientational Coupling between Segments in PDES. Segments in the optimal PDES networks align more readily under stress than what would be expected from the excluded-volume model alone. In these networks, there are comparatively few structural irregularities such as pendent chains or loops. The imperfect networks, in contrast, have many pendent inelastic chains and follow the model predictions reasonably well.

One reasonable explanation is that another factor besides excluded volume can enhance the segment orientation. In the optimal networks, the more efficient orientation could be explained by an enthalpic orientational coupling between segments. In this scenario, the PDES segments are locally aligned with their neighbors in the nondeformed sample. No splitting would be detected in the ^{2}H NMR spectrum because the alignment is local, and the overall distribution of segment orientations is isotropic. The local segment order which was in place before the deformation manifests itself as an increased spectral splitting as segments align with the imposed stress. Thus, the observed ^{2}H NMR splitting involves a contribution from the enthalpic interaction that adds to the order imposed by excluded-volume considerations.

The idea of interacting segments is consistent with the anisotropic motional averaging in PDES indicated by the broad ^{2}H NMR line shapes of amorphous melts and uncompressed PDES networks (as in Figure 5, top). Such a postulate also might explain the shape of the optimal network data in Figure 6. At the onset of deformation, abrupt segment alignment is observed as locally ordered regions shift their directors toward the stress direction. At higher deformations, the excluded-volume effects primarily govern the orientation process. Note that in Figure 6 the limiting slope at high λ for the optimal networks approaches the theoretically predicted slope.

In the case of the imperfect networks, the spectral data in Figure 6 are more typical of conventional elastomers; in fact, they are predicted fairly closely by the model. If an orientational enthalpic coupling contributes to segment alignment, it plays a less significant role for the imperfect networks. The large number of chain ends in our imperfect networks could disrupt the energetic interaction between segments. In addition, the fact that the precursor chains for the imperfect networks were quite short in most cases (see Tables 1 and 2) probably would hinder the energetic coupling, as the nonlinear cross-link points hinder segment−segment alignment. The latter idea is consistent with our observation that mesophase formation in samples under uniaxial extension is hindered by high cross-link density, a result to be discussed in a forthcoming publication.[20] Thus, the proposed idea of an orientational coupling between PDES segments can be justified, even in the light of the rather conventional ^{2}H NMR spectral data obtained for the imperfect PDES samples.

Conclusion

NMR quadrupole splittings have been obtained from PDMS free chains and from elastic network PDES chains in compressed PDES elastomers. The PDES networks are more efficient than previously studied

PDMS networks in orienting PDMS probe chains, a result that follows from the higher chain stiffness of PDES. These results can be interpreted in terms of a model based on excluded-volume interactions between segments. On the other hand, elastic network PDES chains in compressed optimal PDES networks show a substantially higher degree of segment orientation than what is predicted on the basis of excluded-volume arguments alone. This higher degree of orientation and a nonlinear dependence of NMR peak splitting on $(\lambda^2 - \lambda^{-1})$ may be explained in terms of an enthalpic orientational coupling between PDES segments.

Acknowledgment. We acknowledge the National Science Foundation Polymers Program for support under Grants DMR-9706066 and DMR-0078863. Evan McCaskey is grateful for the support of the REU Program of the Cornell Center for Materials Research (CCMR) funded by the National Science Foundation (DMR-9632275). We thank Dr. Kimberly McLoughlin for the synthesis of the deuterated PDMS probe chains.

References and Notes

(1) Brereton, M. G.; Ries, M. E. *Macromolecules* **1996**, *29*, 2644−2651.
(2) Deloche, B.; Samulski, E. T. *Macromolecules* **1981**, *14*, 575−581.
(3) Deloche, B.; Beltzung, M.; Herz, J. *J. Phys., Lett.* **1982**, *43*, 763−769.
(4) Gronski, W.; Stadler, R.; Jacobi, M. *Macromolecules* **1984**, *17*, 741−748.
(5) Toriumi, H.; Deloche, B.; Herz, J.; Samulski, E. *Macromolecules* **1985**, *18*, 304−305.
(6) Jacobi, M.; Stadler, R.; Gronski, W. *Macromolecules* **1986**, *19*, 2884−2887.
(7) Sotta, P.; Deloche, B.; Herz, J.; Lapp, A.; Durand, D.; Rabadeux, J. C. *Macromolecules* **1987**, *20*, 2769−2774.
(8) Dubault, A.; Deloche, B.; Herz, J. *Macromolecules* **1987**, *20*, 2096−2099.
(9) Sotta, P.; Deloche, B. *Macromolecules* **1990**, *23*, 1999−2007.
(10) Jacobi, M.; Abetz, V.; Stadler, R.; Gronski, W. *Polymer* **1996**, *37*, 1669−1675.
(11) McLoughlin, K.; Szeto, C.; Duncan, T. M.; Cohen, C. *Macromolecules* **1996**, *29*, 5475−5483.
(12) McLoughlin, K.; Waldbieser, J. K.; Cohen, C.; Duncan, T. M. *Macromolecules* **1997**, *30*, 1044−1052.
(13) Jarry, J.; Monnerie, L. *Macromolecules* **1979**, *12*, 316−320.
(14) Kornfield, J. A.; Chung, G.; Smith, S. *Macromolecules* **1992**, *25*, 4442−4444.
(15) Brereton, M. G. *Macromolecules* **1993**, *26*, 1152−1157.
(16) Shibanov, Yu. D. *Polym. Sci. U.S.S.R.* **1989**, *31*, 2653−2662.
(17) Kögler, G.; Hasenhindl, A.; Möller, M. *Macromolecules* **1989**, *22*, 4190−4197.
(18) Litvinov, V. M.; Macho, V.; Spiess, H. W. *Acta Polym.* **1997**, *48*, 471−477.
(19) Hedden, R. C.; Saxena, H.; Cohen, C. *Macromolecules* **2000,** *33*, 8676−8684.
(20) Hedden, R. C.; Tachibana, H.; Duncan, T. M.; Cohen, C. Effects of Molecular Structure on Segment Orientation in Siloxane Elastomers: II. NMR Measurements from Stretched Samples. Submitted for publication in *Macromolecules*.
(21) Godovsky, Yu. K. *Angew. Makromol. Chem.* **1992**, *202/203*, 187−212.
(22) Papkov, V. S.; Godovsky, Yu. K.; Svistunov, V. S.; Zhdanov, A. A. *Polym. Sci. U.S.S.R.* **1989**, *31:8*, 1729−1737.
(23) Molenberg, A.; Möller, M. *Macromolecules* **1997**, *30*, 8332−8337.
(24) King, H. S.; Fieser, L. F. *Org. Synth.* **1933**, *13*, 60−65.
(25) Beltzung, M.; Picot, C.; Rempp, P.; Herz, J. *Macromolecules* **1982,** *15*, 1594−1600.
(26) Out, G. J. J.; Klok, H. A.; Möller, M.; Oelfin, D. *Macromol. Chem. Phys.* **1995**, *196*, 195−210.
(27) Hedden, R. C. The effects of molecular structure on the physical properties of poly(diethylsiloxane) elastomers. Ph.D. Thesis, Cornell University, 2000.
(28) Hedden, R. C.; Cohen, C. *Polymer* **2000**, *41*, 6975−6979.
(29) Out, G. J. J.; Turetskii, A. A.; Snijder, M.; Moller, M.; Papkov, V. S. *Polymer* **1995**, *36*, 3213−3221.
(30) Patel, S. K.; Malone, S.; Cohen, C.; Gillmor, J.; Colby, R. H. *Macromolecules* **1992**, *25*, 5241−5251.
(31) Takeuchi, H.; Cohen, C. *Macromolecules* **1999**, *32*, 6792−6799.
(32) Ries, M. E.; Brereton, M. G.; Klein, P. G.; Ward, I. M.; Ekanayake, P.; Menge, H.; Schneider, H. *Macromolecules* **1999**, *32*, 4961−4968.
(33) Godovsky, Yu. K.; Makarova, N. N. *Philos. Trans. R. Soc. London, A* **1994**, *348*, 45−57.
(34) Edwards, S. F. *J. Phys. A* **1975,** *8*, 1670−1680.
(35) Treloar, L. R. G. *The Physics of Rubber Elasticity*; Clarendon Press: Oxford, 1958.
(36) Ries, M. E., personal communication.
(37) Cohen-Addad, J. P. *J. Phys. 1* **1982**, *43*, 1509−1528.
(38) Mark, J. E.; Chiu, D. S.; Su, T.-K. *Polymer* **1978**, *19*, 407−410.
(39) Godovsky, Yu. K.; Volegova, I. A.; Valetskaya, L. A.; Rebrov, A. V.; Novitskaya, L. A.; Rotenburg, S. I. *Polym. Sci. U.S.S.R.* **1988**, *30*, 329−335.
(40) Papkov, V. S.; Kvachev, Yu. P. *Prog. Colloid Polym. Sci.* **1989**, *80*, 221−235.
(41) Godovsky, Yu. K.; Volegova, I. A.; Rebrov, A. V. *Polym. Sci. U.S.S.R.* **1990**, *32*, 726−732.
(42) Godovsky, Yu. K.; Valetskaya, L. A.; Papkov, V. S. *Makromol. Chem., Macromol. Symp.* **1991**, *48/49*, 433−434.

MA0017541